Golden Jackal Optimization Algorithm for Superior Dynamic Performance Control of DC Motors using PID and FOPID Controllers

M. G. Mostafa[1, 2*], N. Z. B. Yahaya[1], I. Shuaibu[1], R. Kannan[1], M. S. Akter[2]

[1]Department of Electrical and Electronics Engineering, Universiti Teknologi PETRONAS, 32610, Perak, Malaysia.
[2]Department of Electrical and Electronic Engineering, World University of Bangladesh, Uttara, Dhaka – 1230, Bangladesh.

ABSTRACT: Direct Current (DC) motors are integral to industrial drive systems due to their efficiency, controllability, and favorable speed-torque characteristics. Achieving optimal speed regulation with PID and FOPID controllers remains challenging, particularly under demanding transient and precision requirements. This study introduces a novel metaheuristic approach, the Golden Jackal Optimizer (GJO), inspired by the cooperative hunting behavior of golden jackals, for the optimal tuning of PID and FOPID controllers. The Integral Time Absolute Error (ITAE) criterion is employed to ensure superior dynamic performance. The proposed GJO-PID and GJO-FOPID controllers were rigorously benchmarked against ten advanced metaheuristic optimization algorithms, including IGWO, PSO, HHO, LHHO, and GOA, across multiple metrics, such as rise time, settling time, overshoot, bandwidth, and phase margin. Results reveal that the GJO controllers surpasses LHHO-FOPID by 6.98%, 4.10%, and 0.56%, and GOA-FOPID by 3.87%, 3.42%, and 0.2022% in faster rise time, shorter settling time, and lower overshoot, respectively. Furthermore, comprehensive sensitivity analyses under varying motor parameters confirm the robustness and reliability of the proposed method. These findings demonstrate the GJO algorithm's ability to deliver superior transient response, stability, and performance, highlighting its potential as a highly effective and generalizable solution for advanced DC motor control in industrial applications.

KEYWORDS: DC motor, Golden Jackal Optimization (GJO) Algorithm, PID controller, FOPID controller, ITAE, Metaheuristics algorithm.

[Received Oct. 31, 2025; Revised Feb. 02, 2026; Accepted Feb. 16, 2026] Print ISSN: 0189-9546 | Online ISSN: 2437-2110

I. INTRODUCTION

Direct Current (DC) motors play a vital role in modern technology due to their precise speed control and efficiency (Ibrahim et al., 2019). They convert electrical energy into mechanical energy, making them essential in applications like handheld tools and consumer electronics. Motor control determines the rotational speed and position (Suman & Giri, 2016), crucial for high-accuracy fields such as robotics and aerospace. Proportional-Integral-Derivative (PID) controllers are commonly used for their accuracy, flexibility, and ease of tuning, thereby enhancing DC motor performance.

Traditional PID tuning methods, such as manual tuning, trial-and-error, and empirical rules like the Ziegler- Nichols method, are limited by their reliance on fixed heuristics, extensive expertise, and simplified assumptions. They often produce suboptimal dynamic responses (e.g., high overshoot, slow settling) because they cannot adapt to complex nonlinearities and parameter variations inherent in DC motor systems (Mosaad et al., 2025). In contrast, metaheuristic optimization algorithms systematically explore a broader parameter space and optimize controller gains based on defined performance criteria, thereby improving transient behavior, reducing overshoot, and enhancing robustness.

Fractional-order PID (FOPID) controllers enhance control of nonlinear systems by incorporating fractional integration and differentiation parameters, offering greater robustness and flexibility than traditional PID controllers. However, proper tuning is crucial for their effectiveness (Das et al., 2011), especially in complex applications like DC motor speed regulation. The fractional order parameters (λ, μ) introduce adjustable memory and damping effects, providing finer tuning flexibility and improved robustness against uncertainties and disturbances.

A substantial body of research confirms that diverse metaheuristic optimization approaches are highly capable and efficient at achieving accurate and reliable tuning of control systems parameters. Unlike traditional algorithms, metaheuristic algorithms employ stochastic search strategies and iterative improvements, effectively exploring the solution space and avoiding local optima. These optimization algorithms have demonstrated superior performance across different real-world engineering design problems, including speed control (Meraj et al., 2020), pipeline monitoring (Ayinla

*Corresponding author: mohammad_22001113@utp.edu.my

doi: http://doi.org/10.63746/njtd.v23i1.4138

et al., 2022), reducing harmonics of multilevel inverters (Islam et al., 2021), energy harvesting control in the oil and gas industry (Mostafa et al., 2006; Mostafa et al., 2024), optimal coreless electrical machine design (Shuaibu et al., 2024), and optimizing power extraction (Akter et al., 2025). Several metaheuristic optimization algorithms, including (Ayinla et al., 2024; Ekinci et al., 2020; Izci & Ekinci, 2023; Li et al., 2021; Munagala & Jatoth, 2021; Rahayu et al., 2022), have been used to optimize the parameters of PID and FOPID controllers for regulating the speed of DC motors.

Despite extensive research on DC motor speed control using classical and metaheuristic-based controllers, to the best of our knowledge, no prior studies have investigated the application of the Golden Jackal Optimizer (GJO) for this purpose. In particular, the collaborative hunting-and-pouncing strategy of GJO effectively mitigates premature convergence and avoids local optima, while its cooperative leader–follower mechanism enhances population diversity and guides search agents toward promising regions, thereby improving solution accuracy and increasing the likelihood of attaining the global optimum relative to random-based optimization techniques. However, these distinctive advantages of GJO have not yet been explored in the context of DC motor speed regulation. Addressing this research gap, the present study proposes the design of GJO-based PID and FOPID controllers optimized using the ITAE objective function to enhance speed regulation performance and robustness. A comprehensive analysis, including step-response, stability, and sensitivity evaluations, is conducted to assess system behavior under varying operating conditions. A detailed analysis, including step-response, stability, and sensitivity analyses, was conducted to assess the plant's behavior under varying parameter conditions. The unique contribution of the study can be summarized as follows in threefold:

- This work presents the utilization of the GJO-based algorithm to optimally tune the parameters of the PID and FOPID controllers for regulating the DC motor's speed.
- The performance of the suggested GJO-based PID and FOPID controllers was thoroughly examined through rigorous assessments of convergence profiles, step and frequency response analyses, and disturbance sensitivity analyses.
- The suggested GJO-PID and GJO-FOPID controllers demonstrate enhanced performance compared with existing and recently proposed (IGWO-PID (Li et al., 2021), IGWO-FOPID (Li et al., 2021), PSO-PID (Rahayu et al., 2022), PSO-FOPID (Rahayu et al., 2022), HHO-PID (Ekinci et al., 2020), HHO-FOPID (Munagala & Jatoth, 2021), LHHO-PID (Ayinla et al., 2024), LHHO-FOPID (Ayinla et al., 2024), Gazelle Optimization Algorithm (GOA)-PID (Izci & Ekinci, 2023), GOA-FOPID (Izci & Ekinci, 2023)) controllers for speed control of DC motors.

II. RELATED WORK ON DC MOTOR CONTROL

Numerous investigations have explored the use of metaheuristic optimization methods to tune PID and FOPID controllers for DC motor speed regulation, with the ITAE objective function commonly favored for its superior performance in improving transient response. The authors (Hekimoğlu, 2019) proposed atom search optimization (ASO) and its chaotic variant (ChASO) for optimal FOPID tuning with respect to ITAE and ITSE. While ITSE tends to penalize initial errors and may induce aggressive control actions and overshoot, ITAE provides a more balanced response by emphasizing sustained error reduction, leading to faster settling and reduced oscillations. Furthermore, the work by (Ekinci et al., 2021) employed opposition-based learning–enhanced Henry gas solubility optimization (OBL/HGSO) to tune PID controllers using ITAE, achieving superior transient performance, robustness, and disturbance rejection compared with several metaheuristic-based controllers. However, the study is limited to PID controllers and does not investigate FOPID controllers.

The study by (Ekinci et al., 2020) applied Harris Hawk Optimization (HHO) algorithm for DC motor control and optimization, with ITAE adopted due to its ability to suppress sustained errors and improve transient performance. The proposed controllers achieved a balanced trade-off among rise time, settling time, and overshoot. The Particle Swarm Optimization (PSO) algorithm was used by (Rahayu et al., 2022) to tune PID controllers, yielding more stable results than conventional approaches. Nevertheless, its main limitations include early convergence, getting trapped in local optima, and challenges in balancing global exploration with local exploitation (Kumar et al., 2023; Qaraad et al., 2024).

The Grey Wolf Optimizer (GWO) and its hybrids, such as GWO-PI and GWO-RUN (Younus et al., 2023), (Kumari & Kumar, 2023) have been used to improve speed tracking and robustness against parameter variations and disturbances. They effectively enhance global search capability and controller performance. Yet, GWO-based methods can exhibit slow convergence and limited avoidance of local optima, reducing overall efficiency for dynamic DC motor control. Another study by (Agarwal et al., 2018) also used GWO–based FOPID controllers with ITAE, demonstrating improved rise and settling times, comparable overshoot, and robust performance under parameter variations. To further enhance the performance of the GWO-based scheme, (Li et al., 2021) propose IGWO, which demonstrates robustness in fault diagnosis and parameter optimization. However, it suffers from slow convergence, limiting its effectiveness for real-time DC motor control. The Leader HHO (LHHO) algorithm (Ayinla et al., 2024) and the hybrid AOA-HHO algorithm (Issa, 2023), both based on ITAE, improve transient performance and tuning for PID/FOPID controllers, yielding superior rise time, settling time, and overshoot. Similarly, the GOA (Izci & Ekinci, 2023) enhances the performance of the FOPID controller, achieving accurate motor regulation.

Although these metaheuristic algorithms deliver significant performance improvements, challenges such as slow convergence, trapping in local optima, and the need to balance exploration and exploitation continue to motivate the use of more advanced approaches, such as GJO. In this study, the GJO algorithm is employed for controller tuning due to its strong global search capability, adaptive exploration–exploitation balance, and fast convergence, which are well-suited to nonlinear and disturbance-prone DC motor control systems (Chopra & Ansari, 2022; Podlubny, 1994). Its cooperative hunting mechanism enables efficient exploration

of the search space while avoiding premature convergence, thereby enabling reliable identification of optimal controller parameters. In this study, both GJO-based PID and FOPID controllers are evaluated for comprehensive performance comparisons. While PID ensures simplicity, FOPID provides enhanced flexibility, robustness, and improved transient response.

III. DC MOTOR MODELLING

The industry commonly uses Brushless DC (BLDC) motors to regulate armature voltage and speed. This paper examines the application of BLDC for this purpose, which comprises two primary control sections: the field and armature (Ayinla et al., 2023). The diagram in Figure 1 illustrates the electrical circuit corresponding to the armature and a schematic representation of the forces acting on the rotor.

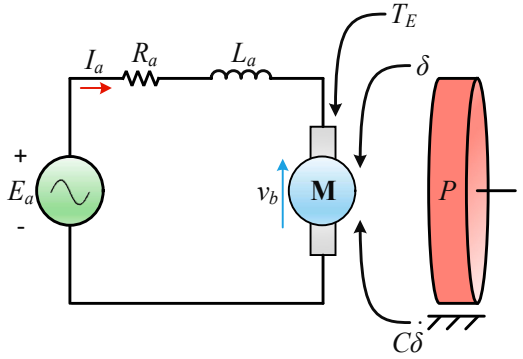

Figure 1 Brushless DC motor's equivalent circuit

Regulating the speed of a DC motor is commonly achieved by adjusting the armature voltage (E_a). This voltage generates an electro-mechanical force that corresponds to the current (I_a) flowing within the circuit and is directly proportional to the rotational speed (δ) (Ayinla et al., 2024). We can realize the differential equation for the armature circuit by applying Kirchhoff's Voltage Law (KVL) to Figure 1, as shown in Equation (1). The angular velocity (Ω) and the motor's induced voltage (v_b) are directly proportional whilst the magnetic flux is constant, as described in Equation (2).

$$E_a = I_a r_a + l_a \frac{dI_a}{dt} + v_b \tag{1}$$

$$v_b = M_b \frac{d\delta}{dt} = M_b \Omega \tag{2}$$

The sum of frictional and inertia torques equal the torque produced by the armature current, leading to the overall torque, as illustrated in Equation (3).

$$T_E - T_l = P\frac{d\Omega}{dt} + C\Omega = M_m I_a \tag{3}$$

Here, the variables I_a, E_a, L_a *and* R_a, represent the applied current, voltage, inductance, and resistance of the DC motor armature, which are measured in volt (V), ampere (A), ohm (Ω), and Henry (H), accordingly. In addition, v_b and M_b represent the back electromotive force and constant, measured in volts (V) and volts-second per radian ($V.s/rad$), respectively. Furthermore, δ and Ω represent the angular speed and velocity of the motor shaft in radians per second (rad/s) units. T_E, T_l and P correspondingly represent the motor's electric torque, load torque, and moment of inertia, measured in newton-meters ($N.m$) and kilogram-square meters (kg.m^2). Finally, M_m and C represent torque constant and the frictional loss of the motor in the unit of $N.m/A$ and $N.m.s/rad$, respectively. Incorporating the Laplace transform and assuming zero initial conditions for Equations (1-3), we obtain Equation (4-6).

$$E_a(s) = (L_a + R_a)I_a(s) + V_b(s) \tag{4}$$

$$V_b(s) = M_b\Omega(s) \tag{5}$$

$$T_E(s) - T_l(s) = (Ps + C)\Omega(s) = M_m I_a(s) \tag{6}$$

After replacing Equation (5) with Equation (4) and shortening Equation (4) and Equation (6), we deduce Equation (7) and Equation (8).

$$I_a(s) = \frac{E_a(s) - M_b\Omega(s)}{(L_a s + R_a)} \tag{7}$$

$$\Omega(s) = \frac{T_E(s) - T_l(s)}{(Ps + C)} = \frac{M_m}{(Ps + C)} I_a(s) \tag{8}$$

A schematic of the BLDC motor arrangement is shown in Figure 2. The transfer function that links the input voltage $E_a(s)$ to the output motor speed $\Omega(s)$ of the DC motor when there is no load torque is expressed in Equation (9). However, in real industrial settings, load torque exists and often exhibits dynamic behavior due to sudden process disturbances. The value of the parameters specified in Table 1 was used to conduct the simulation (Ayinla et al., 2024; Kumari & Kumar, 2023). By substituting these numbers into Equation (9), we derive Equation (10); Equation (11) follows from further simplification.

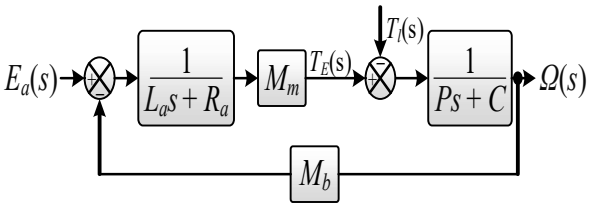

Figure 2 A schematic diagram depicting the arrangement of a BLDC motor

$$G_p(s) = \frac{\Omega(s)}{E_a(s)} = \frac{M_m}{(L_a s + R_a)(Ns + C) + M_b M_m} \text{ for } T_l = 0 \tag{9}$$

$$G_P(s) = \frac{0.015}{(2.7s + 0.4)(0.0004s + 0.0022) + 0.00075} \tag{10}$$

$$G_p(s) = \frac{15}{1.08s^2 + 6.1s + 1.63} \tag{11}$$

Table 1 The simulation parameters of the DC motor

#	Parameters	Value
1	P	0.0004 kg.m^2
2	L_a	2.7 H
3	C	0.0022 N.m. s/rad
4	M_m	0.015 N.m/A
5	M_b	0.05 V. s
6	R_a	0.4 Ω

A. DC Motor Speed Control via Controllers

In control engineering, controllers link the current process state to the desired setpoint, improving steady-state accuracy and response time (Issa, 2023). Common controllers for DC motor speed control include PID and FOPID, as illustrated in the block diagram in Figure 3.

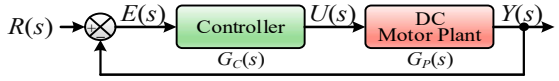

Figure 3 Diagram illustrating the components and connections of a DC motor with a controller

1) DC Motor Speed Control via PID Controller

PID controllers are widely used in process control industries due to their numerous advantages. Their stability analysis is remarkably straightforward, and they can be easily adjusted. PID control is based on a closed-loop feedback system that aims to minimize the error between the output and the desired setpoint. Equations (12) and (13) present the time-domain formulation of a PID controller and its equivalent transfer function. Equation 14 depicts the closed-loop transfer function of the DC motor with unity feedback and a PID controller, as obtained from Figure 4a. By substituting $G_P(s)$ and $G_{DC-PI}\ (s)$ in Equations (9) and (13) into Equation (14), we obtain Equation (15).

$$u(t) = K_p e(t) + K_i \int e(t) + K_d \frac{d}{dt} e(t) \quad (12)$$

$$G_{PID}(s) = K_p + \frac{K_i}{s} + K_d s = K_p + K_i s^{-1} + K_d s \quad (13)$$

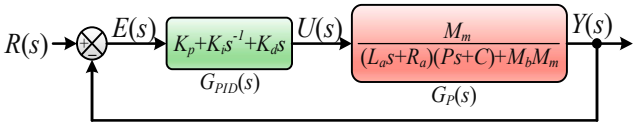

Figure 4a A block diagram that depicts the regulation of a DC motor using a PID-based controller

$$G_{DC-PID}(s) = \frac{G_{PID}(s) \times G_P(s)}{1 + [G_{PID}(s) \times G_P(s)]} \quad (14)$$

$$G_{DC_{PID}}(s) = \frac{M_m(K_p + K_i s^{-1} + K_d s)}{[(Ps+C)(L_a s + R_a) + M_b M_m + M_m(K_p + K_i s^{-1} + K_d s)]} \quad (15)$$

2) DC Motor Speed Control via FOPID Controller

The FOPID controller features two additional finely adjusted parameters (λ, μ) compared to standard PID controllers, enabling it to maintain stability against variations in the controlled system and the controller itself (Izci & Ekinci, 2023). Equation (16) provides the time-domain form of an FOPID controller, whereas Equation (17) gives its transfer function.

$$u(t) = K_p e(t) + K_i D_t^{-\lambda} e(t) + K_d D_t^{\mu} e(t) \quad (16)$$

$$G_{FOPID}(s) = K_p + K_i s^{-\lambda} + K_d s^{\mu} \quad (17)$$

The desired signal is represented by $u(t)$, whereas the error signal is denoted by $e(t)$. The operators $D_t^{-\lambda}$ and D_t^{μ} correspond to the integral and differential operations associated with fractional order, respectively.

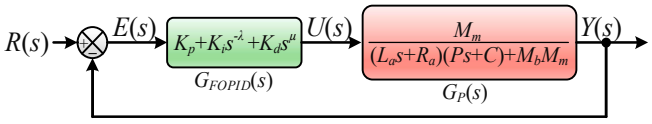

Figure 4b A block diagram that depicts the regulation of a DC motor using a FOPID-based controller

Similarly, as shown in Figure 4b, Equation (18) represents the transfer function of a DC motor controlled by a FOPID controller with unity feedback.

$$G_{DC-FOPID}(s) = \frac{G_{FOPID}(s) \times G_P(s)}{1 + \{G_{FOPID}(s) \times G_P(s)\}} \quad (18)$$

We obtain Equation (19) by substituting the $G_p(s)$ and $G_{FOPID}(s)$ in Equation (9) and Equation (17) into Equation (18).

$$G_{P_{FOPID}}(s) = \frac{M_m(K_p + K_i s^{-\lambda} + K_d s)}{[(Ps+C)(L_a s + R_a) + M_b M_m + M_m(K_p + K_i s^{-\lambda} + K_d s^{\mu})]} \quad (19)$$

IV. GOLDEN JACKAL OPTIMIZATION (GJO) ALGORITHM

A widely used method for optimizing PID and FOPID controllers in control systems involves metaheuristic optimization algorithms. While many nature-inspired algorithms have been used to tune DC motor-based controllers, research has not yet thoroughly explored GJO. This algorithm leverages the cooperative hunting strategies of golden jackals, which hunt in pairs or packs, to achieve effective control of DC motor speed. This technique, introduced by (Chopra & Ansari, 2022), emulates the golden jackal's hunting strategy, a fascinating example of their cooperative behavior. The primary phases of GJO can be divided into three categories. First, the pair engages in a collaborative search-and-detection phase, utilizing visual scanning and auditory cues to locate potential prey. Once identified, they work together to herd and encircle the target, limiting its escape options through coordinated movements. This cooperative herding and encirclement are followed by an agitation and immobilization stage, where the jackals further stress and weaken the prey through harassing behaviors. Finally, when the prey is sufficiently immobilized, one of the

jackals delivers a decisive predatory strike to secure the kill. The golden jackal's cooperative hunting strategy can be further divided into three distinct phases:

- Search space definition phase: The jackals collaborate to establish a search area to identify potential prey locations.
- Exploration phase: Once prey is identified, the jackals work together to locate, perceive, and follow the target. This phase may involve coordinated movements and adjustments to the search pattern in response to the prey's behavior.
- Exploitation phase: The exploitation phase begins when jackals successfully track their prey, limiting its escape, then herding and stressing it before launching a final, coordinated attack to immobilize it.

A. Search Space Definition

The initial solution (S_0) is generated randomly to establish the population of golden jackals within the search area. This utilizes a uniform random vector ($rand$) which ranges from 0 to 1. The initialization considers the lower boundary (S_L) and the upper boundary (S_U) of the search space, as described by Equation (20).

$$S_0 = S_L + rand(S_U - S_L) \tag{20}$$

The initialization generated from Equation (20) can be arranged in matrix form to determine the initial position of the prey ($\boldsymbol{P}_*$) as provided in Equation (21), where S_{mn} is the n-th dimension of the m-th prey.

$$\boldsymbol{P}_* = \begin{bmatrix} S_{11} & S_{12} & \dots & S_{1v} \\ S_{21} & S_{22} & \dots & S_{2v} \\ . & . & . & . \\ . & . & . & . \\ S_{p1} & S_{p2} & \dots & S_{pv} \end{bmatrix} \tag{21}$$

The notations p and v represent the total number of prey and the variable for the search space size, respectively. The fitness function (ϑ) of each prey is evaluated throughout the optimization phase. This function determines the quality of each solution and guides the process as computed in Equation (22).

$$\vartheta = \begin{bmatrix} f(S_{11}, S_{12}, \dots\dots\dots S_{1v}) \\ f(S_{21}, S_{22}, \dots\dots\dots S_{2v}) \\ . \\ . \\ . \\ f(S_{p1}, S_{p2}, \dots\dots\dots S_{pv}) \end{bmatrix} \tag{22}$$

The matrix in Equation (22) indicates prey fitness values; the highest fitness jackal becomes the Male Jackal leader, while the second highest is the Female Jackal, collaborating for successful hunting.

B. Exploration phase (Prey Searching)

Golden jackals use a coordinated hunting strategy, adapting their roles in response to environmental conditions. If unsuccessful, they explore alternative prey, with dynamic positioning throughout the search process described in Equations (23) and (24), respectively.

$$S_1(t) = S_{male}(t) - E_p \,.\, |S_{male}(t) - \varpi.\boldsymbol{P}_*(t)| \tag{23}$$

$$S_2(t) = S_{female}(t) - E_p \,.\, |S_{female}(t) - \varpi.\boldsymbol{P}_*(t)| \tag{24}$$

In the Equations t indicates the current iteration, S_1 and S_2 represent the updated locations for both the male and female jackals, respectively. S_{male} and S_{female} denote the current locations of the male and female jackals, respectively. The energy of the prey (E_p) is determined based on the initial energy (E_{p0}), the maximum iterations (T), and the current iteration (t) as described in Equation 25.

$$E_p = 1.5\left(1 - \frac{t}{T}\right) . E_{p0} \tag{25}$$

Here, E_p represents the energy of the prey, and ϖ is the Lévy movement. In Equations (23) and (24), the concept of Lévy movement is represented by (ϖ) as introduced to model the prey's trajectory. The movement is influenced by the Lévy flight (LF) distribution. The Lévy movement is an arbitrary random vector that captures the inherent randomness in the prey's movement. The product of the Lévy movement and the prey position in these equations represents the prey's movement pattern under Lévy flight behavior (Mantegna, 1994), and the Lévy movement (ϖ) is calculated using Equation (26).

$$\varpi = 0.05 \times LF(s) \tag{26}$$

The LF distribution is given as presented in Equation (27).

$$LF(S) = 0.01 \times \frac{\eta \times \psi}{\left|\aleph^{\frac{1}{\alpha}}\right|};$$

$$\psi = \left(\frac{\Gamma(1+\alpha)\times\sin\left(\frac{\pi\alpha}{2}\right)}{\Gamma\left(\frac{1+\alpha}{2}\right)\times\alpha\times\left(2^{\frac{\alpha-1}{2}}\right)}\right) \tag{27}$$

where η, $\aleph$ are random numbers, and they are drawn from a normal distribution with η having a standard deviation of ψ and $\aleph$ having a standard deviation of 1. The parameter α is usually taken as 1.5.

C. Exploration Phase (Prey Enclosing and Pouncing)

In this phase, persistent harassment by the jackal pair reduces the prey's ability to escape. This compromised state enables the jackals to successfully encircle the previously located prey. This behavioral pattern exhibited by male and female jackals is represented mathematically in Equations (28) and (29), respectively.

$$S_1(t) = S_{male}(t) - E_p \,.\, |\varpi.S_{male}(t) - P_*(t)| \tag{28}$$

$$S_2(t) = S_{female}(t) - E_p \,.\, |\varpi.S_{female}(t) - P_*(t)| \tag{29}$$

The mean of Equations (23) and (24), as presented in Equation (30), gives the updated jackal positions.

$$S(t+1) = \frac{S_1(t)+S_2(t)}{2} \tag{30}$$

D. Transitioning from exploration to the exploitation phase

A decrease in prey energy (E_p) prompts jackals to attack, whereas an increase leads them to explore new prey, as detailed in the GJO algorithm, as expressed in Equation (31). The pseudocode for the GJO algorithm is provided in

Algorithm 1. Figure 5 illustrates the sequential process of the algorithm.

$$Transition(S) = \begin{cases} Exploration, & |E_p| > 1 \\ Exploitation, & |E_p| < 1 \end{cases} \quad (31)$$

Algorithm 1: Pseudo-code of GJO Algorithm

/*initialization*/

Input: Population size (N), controller dimension (D), maximum iteration t_{max}, lower (S_L) and upper boundary (S_U) search space

Output: Prey position and its best fitness value

Generate a random position vector: S_{mn} of the m-th prey with the n-th dimension at $t = 1$

Begin

While $t \leq t_{max}$ **do**

Evaluate the fitness values of prey

S_1 = best prey (Male Jackal position)

S_2 = second best prey (Female Jackal position)

For each prey

Update the evading energy (E_p) using Eq. (25)

Update the prey trajectory with Lévy movement (ϖ) using Eq. (26) and Eq. (27)

/*exploration stage*/

If evading energy $|E_p| \geq 1$ **do**

Update the prey position using Eq. 23, Eq. 24, and Eq. 30

/*exploitation stage*/

else if evading energy $|E_p| < 1$ **do**

Update the prey position using Eq. 28, Eq. 29, and Eq. 30

end if

End for

Set $t = t + 1$

End while

Return the best solution S_1

End

E. Proposed GJO-based PID/FOPID Controller

The proposed GJO technique was used to optimize integer (K_p, K_i, K_d) and fractional-order (K_p, K_i, K_d, λ *and* μ) controllers' parameters. The PID controller parameters (K_p, K_i, K_d) were bounded between 0.001-20, while the fractional-order parameters (λ, μ) were constrained between 0 and 1, as presented in Table 2. The error value of the DC motor output was evaluated after each iteration and applied to the relevant ITAE objective function. ITAE prioritizes error elimination in transient response, promoting faster settling and reduced oscillations in DC motor speed control. In contrast, ITSE penalizes initial errors, which can lead to aggressive control actions and overshoot, making ITAE a more balanced choice for control objectives (Hekimoğlu, 2019). Additionally, the ITAE-based objection function enables the synthesis of controllers that achieve a fast rise time, minimal overshoot, rapid settling, and negligible steady-state error, which are essential for high-performance DC motor speed control. These advantages explain the widespread adoption of ITAE in recent metaheuristic optimization-based controller design and justify its selection as the primary objective function in this work. Figure 6 presents the block diagram of the proposed GJO-based FOPID controller for regulating DC motor speed.

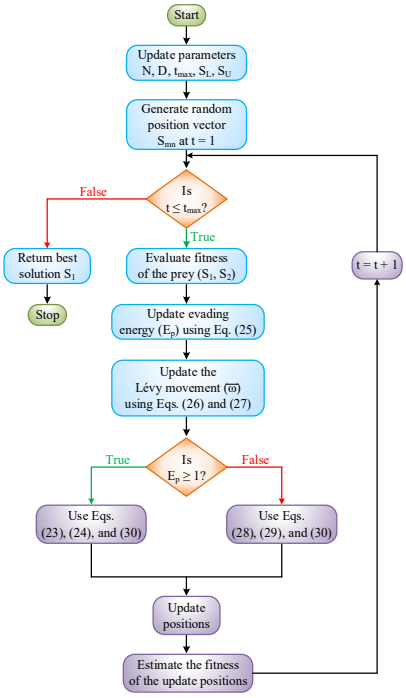

Figure 5 Flowchart of the proposed GJO algorithm-based speed control DC motor

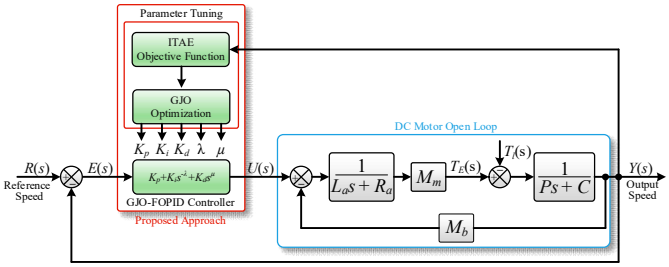

Figure 6 Block diagram of the proposed DC Motor with GJO-FOPID Controller

Table 2 details the parameters of the employed metaheuristics optimization algorithm. These parameters, including the population size, iterations, Lévy flight, and lower-upper parameter bounds was selected based on prior studies demonstrating that this value provides an effective balance between local intensification and global diversification, leading to improved search efficiency and convergence stability (Ayinla et al., 2024; Eker et al., 2021; Hekimoğlu, 2019).

The fractional-order integrator $s^{-\lambda}$ and differentiator s^{μ} in the FOPID controller was implemented using the Oustaloup approximation, which is widely adopted for fractional-order control simulation in time-domain analysis [ref]. The approximation was realized over the frequency range $[10^{-2}, 10^{2}]$ rad/s using a 5th-order recursive filter, which provides a good trade-off between approximation accuracy and computational efficiency. The frequency response, as shown in the Bode plot, was obtained by substituting $s = jw$ in the fractional-order terms $s^{-\lambda}$ and s^{μ}, which yield magnitude responses proportional to $\omega^{-\lambda}$ and ω^{μ} and

constant phase shifts of $-\lambda \times 90\circ$ and $\mu \times 90\circ$, respectively.

Table 2 Parameters of the proposed GJO-based PID/FOPID Algorithm

Variables	Value
Jackal population size (N)	50
Iterations as number (t_{max})	50
Levy flight constant (β)	1.5
PID/FOPID controller dimension (D)	3/5
Levy movement constant (ϖ)	0.0075
Lower limits (S_l) ($K_p, K_i, K_d, \lambda, \mu$)	[0.001 0.001, 0.001 0 0]
Upper limits (S_u) ($K_p, K_i, K_d, \lambda, \mu$)	[20 20 20 1 1]
Simulation time (t_{sim})	0.5 s

V. SIMULATION RESULTS AND DISCUSSION

This section presents the simulated results for both the GJO-PID and GJO-FOPID controllers. To assess the effectiveness and superiority of the proposed controllers (GJO-PID and GJO-FOPID), their performance was evaluated against two recently proposed GOA-PID/FOPID and LHHO-PID/FOPID metaheuristic optimization-based controllers, as well as three other existing controllers (IGWO-PID/FOPID, PSO-PID/FOPID, and HHO-PID/FOPID). The comparisons are based on convergence, step-response, frequency-response, and sensitivity analyses.

A. Convergence Plots of the Proposed GJO and Existing Algorithm

The convergence plot is a curve used to evaluate the effectiveness of metaheuristic optimization algorithms. It illustrates the improvement in the objective function value (i.e., the best fitness value) on the y-axis as a function of the number of iterations on the x-axis. Table 3 compares the convergence behaviors of six (6) metaheuristic optimization algorithms for ITAE-based PID and FOPID-controlled DC motors for 50 iterations. In the PID category, as shown in Figure 7, GOA, PSO, and LHHO converge after thirty-one (31), twenty-five (25), and fifteen (15) iterations, respectively. Though HHO converges after the five (5) iterations, it has a higher fitness value. The proposed GJO and IGWO converge after eleven (11) iterations, but the proposed exhibits a better fitness function value.

Table 3 Optimal ITAE objective function values for various controllers

#	Algorithm	Objective Function (ITAE)
1	IGWO-PID (Li et al., 2021)	0.00315876
2	PSO-PID (Rahayu et al., 2022)	0.0031712
3	HHO-PID (Ekinci et al., 2020)	0.0031712
4	LHHO-PID (Ayinla et al., 2024)	0.0031614
5	GOA-PID (Izci & Ekinci, 2023)	0.0031571
6	GJO-PID (Proposed)	0.0029194
7	IGWO-FOPID (Li et al., 2021)	0.0012002
8	PSO-FOPID (Rahayu et al., 2022)	0.0012007
9	HHO-FOPID (Munagala & Jatoth, 2021)	0.0015378
10	LHHO-FOPID (Ayinla et al., 2024)	0.0013796
11	GOA-FOPID (Izci & Ekinci, 2023)	0.0012567
12	GJO-FOPID (Proposed)	0.0011636

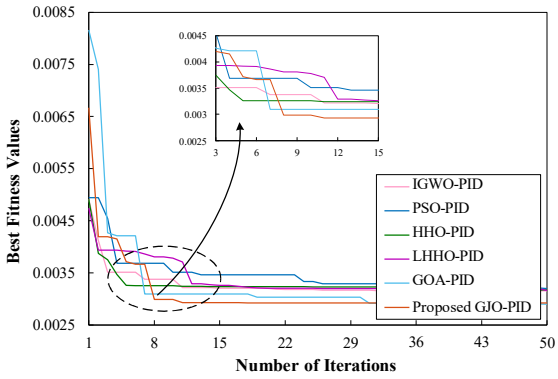

Figure 7 Proposed GJO and their baseline PID controllers-based convergence curve for the ITAE Objective function

Figure 8 presents the convergence curve of the proposed GJO-FOPID controller. The GJO-FOPID controller demonstrates superior convergence performance compared with five other FOPID controllers, achieving the lowest fitness value of 0.0011636 after seven iterations. In contrast, HHO-FOPID and PSO-FOPID showed the worst performance, converging after forty (40) iterations, whereas IGWO-FOPID, LHHO-FOPID, and GOA-FOPID performed better but were still slower than GJO-FOPID. The proposed controller achieves superior convergence performance through the GJO's collaborative hunting–pouncing strategy and leader–follower cooperation, which prevent premature convergence, maintain population diversity, and effectively guide the search toward the global optimum, outperforming random-based methods such as PSO.

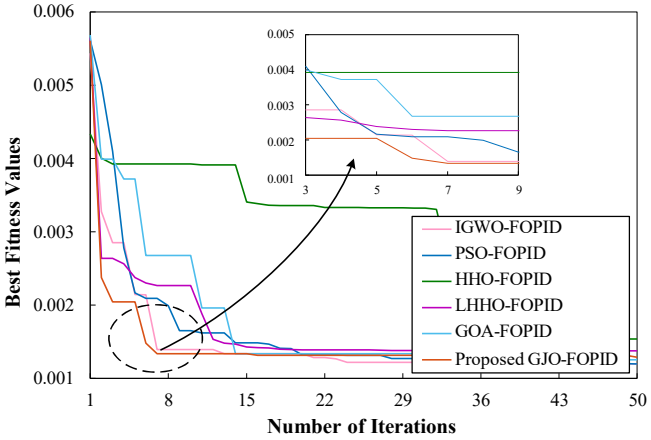

Figure 8 Proposed GJO and their baseline FOPID controllers-based convergence curve for the ITAE Objective function

B. Step Response Analysis

This subsection presents a detailed analysis of the response of the proposed GJO PID and FOPID controllers to a step input. This study yields important insights into the dynamic characteristics of DC motor-based control systems, including critical parameters such as rise time (t_r), settling time (t_s), percentage overshoot (O_p), steady-state error (E_{SS}), and peak value (p_v). The response to a step input is a crucial aspect of control system design, as it determines how quickly

and accurately the system can adjust to changes in the reference signal.

$$G_{DC\_PID}(s) = \frac{0.050 \quad ^{2}+0.3000s \quad .08567}{0.00108 \ ^{3}+0.05693s^{2}+0.3016s \quad .08567} \quad (32)$$

$$G_{DC\_FOPID}(s) = \frac{0.10 \quad ^{1.1625}+0.3s^{0.1906}+0.2999}{0.0011s^{2.1906}+0.0061s^{1.1906}+0.1040 \ ^{1.1625}+0.3016s^{0.1906}+0.2999} \quad (33)$$

Table 4 presents the optimal values for each fine-tuned parameter of the PID and FOPID controllers, obtained by applying the proposed GJO algorithm and other state-of-the-art methods. Equations (32) and (33) express the corresponding transfer functions for the proposed GJO-PID controller and its FOPID counterparts of the DC motor systems. The step response results of the proposed GJO-PID/FOPID controllers are compared with ten (10) existing controllers, namely IGWO-PID, IGWO-FOPID, PSO-PID, PSO-FOPID, HHO-PID, HHO-FOPID, and the recently proposed LHHO-PID, LHHO-FOPID, GOA-PID, and GOA-FOPID controllers in Table 5.

Table 4 Proposed GJO-PID/FOPID with other compared controller gain parameters

#	Algorithm	Controllers gain parameters				
		K_p	K_i	K_d	λ	μ
1	IGWO-PID (Li et al., 2021)	19.99	5.39	3.36	-	-
2	PSO-PID (Rahayu et al., 2022)	20.00	5.51	3.30	-	-
3	HHO-PID (Ekinci et al., 2020)	20.00	5.53	3.37	-	-
4	LHHO-PID (Ayinla et al., 2024)	19.98	5.40	3.36	-	-
5	GOA-PID (Izci & Ekinci, 2023)	20.00	5.43	3.36	-	-
6	GJO-PID (Proposed)	20.00	5.71	3.39	-	-
7	IGWO-FOPID (Li et al., 2021)	19.95	19.93	19.99	0.73	0.59
8	PSO-FOPID (Rahayu et al., 2022)	20.00	19.49	20.00	0.75	0.58
9	HHO-FOPID (Munagala & Jatoth, 2021)	13.65	19.99	5.94	0.18	0.96
10	LHHO-FOPID (Ayinla et al., 2024)	19.41	18.14	6.79	0.28	0.95
11	GOA-FOPID (Izci & Ekinci, 2023)	19.72	18.76	6.71	0.22	0.96
12	GJO-FOPID (Proposed)	20.00	20.00	6.94	0.19	0.97

Table 5 Step response of the proposed with various alternative controller approaches

#	Algorithm	t_r (s)	t_s (s)	O_p (%)	E_{SS}	p_v (rad/s)
1	IGWO-PID (Li et al., 2021)	0.0463	0.0800	0.2382	5.3e-04	1.0029
2	PSO-PID (Rahayu et al., 2022)	0.0467	0.0801	0.3228	7.7e-04	1.0040
3	HHO-PID (Ekinci et al., 2020)	0.0462	0.0800	0.2145	6.2e-04	1.0028
4	LHHO-PID (Ayinla et al., 2024)	0.0462	0.0800	0.2322	5.3e-04	1.0029
5	GOA-PID (Izci & Ekinci, 2023)	0.0462	0.0799	0.2348	5.6e-04	1.0029
6	GJO-PID (Proposed)	0.0460	0.0801	0.1779	7.4e-04	1.0025
7	IGWO-FOPID (Li et al., 2021)	0.0268	0.1286	16.954	0.004	1.1642
8	PSO-FOPID (Rahayu et al., 2022)	0.0274	0.1293	17.905	0.005	1.1737
9	HHO-FOPID (Munagala & Jatoth, 2021)	0.0307	0.0505	0.6109	0.001	1.0049
10	LHHO-FOPID (Ayinla et al., 2024)	0.0276	0.0457	0.9654	0.001	1.0084
11	GOA-FOPID (Izci & Ekinci, 2023)	0.0268	0.0454	0.6128	0.001	1.0050
12	GJO-FOPID (Proposed)	0.0258	0.0439	0.4087	0.0010	1.0030

The step response of the proposed GJO-PID and GJO-FOPID controllers is compared with state-of-the-art controllers, including the recently proposed (LHHO-PID (Ayinla et al., 2024), LHHO-FOPID (Ayinla et al., 2024), GOA-PID (Izci & Ekinci, 2023), GOA-FOPID (Izci & Ekinci, 2023), as well as other controllers such as IGWO-PID (Li et al., 2021), IGWO-FOPID (Li et al., 2021), PSO-PID (Rahayu et al., 2022), PSO-FOPID (Rahayu et al., 2022), HHO-PID (Ekinci et al., 2020) and, HHO-FOPID (Munagala & Jatoth, 2021), as presented in Table 5.

The GJO-PID shows the fastest rise time (t_r) at 0.0460 s, followed closely by GOA-PID and HHO-PID at 0.0462 s. In the FOPID category, GJO-FOPID excels with a rise time of 0.0258 s, while HHO-FOPID takes the longest at 0.0307 s. The proposed GJO-FOPID responds quickly to input signals by 3.87%, 6.20%, 18.99%, 6.98%, and 3.87% compared to IGWO-FOPID, PSO-FOPID, HHO-FOPID, LHHO-FOPID, and GOA-FOPID, respectively. This improvement indicates that the proposed GJO PID and GJO-FOPID exhibit better dynamic performance in rise time than the existing methods.

The proposed GJO-FOPID outperforms other controllers in settling time (t_s), achieving 0.0439 s compared to GOA-FOPID (0.0454 s), LHHO-FOPID (0.0457 s), and HHO-FOPID (0.0505 s). It converges significantly faster than IGWO-FOPID and PSO-FOPID, indicating superior stability relative to most existing control methods. For overshoot, PSO-PID has the maximum overshoot (O_p) of 0.3228%; this is followed by IGWO-PID, GOA-PID, and LHHO-PID, with overshoots of 0.2382%, 0.2348%, and 0.2322%, respectively. The performance of HHO-PID in terms of overshoot is closest to that of the proposed GJO-PID, with a value of 0.2145%. GJO-PID shows the best performance, with the least overshoot of 0.1779%. However, the step response results in Table 5 indicate a performance trade-off: for example, although the GJO-PID controller exhibits a marginally longer settling time (0.0801 s) compared to GOA-PID (0.0799 s).

Likewise, in FOPID control, the GJO-FOPID method demonstrates superior performance, exhibiting an overshoot of only 0.4087%. In contrast, PSO-FOPID and IGWO-FOPID exhibit the worst performance, with maximum overshoots of 17.9054% and 16.9840%, respectively. The maximum overshoots in GOA-FPOID and HHO-FOPID are similar, with values of 0.6128% and 0.6109%, whereas LHHO-FOPID has an overshoot of 0.9654%. Consequently, the proposed GJO-FOPID outperforms the compared methods by 16.5453%, 17.4967%, 0.2022%,0.5567%, and 0.2041% for IGWO-FOPID, PSO-FOPID, HHO-FOPID, LHHO-FOPID, and GOA-FOPID, respectively.

As shown in Table 5, the proposed controllers exhibit stability and precision, with minimal errors between the setpoint and the actual output during signal changes. Additionally, considering steady-state error (E_{ss}), the proposed GJO-PID and GJO-FOPID controllers demonstrate the lowest oscillation before settling down to their final steady state, with peak values (p_v) of 1.0025 rad/s, and 1.0030 rad/s, respectively.

The GJO-PID and GJO-FOPID controllers exhibit superior performance in terms of minimal overshoot, peak value, and shorter settling and rise times compared with recent and state-of-the-art controllers, as shown in Figures 9 and 10. The investigation shows that the suggested controllers demonstrate exceptional performance, not only with recently proposed controllers LHHO-PID (Ayinla et al., 2024), LHHO-FOPID (Ayinla et al., 2024), GOA-PID (Izci & Ekinci, 2023), and GOA-FOPID (Izci & Ekinci, 2023) controllers but also with other cutting-edge PID/FOPID controllers like IGWO, PSO, and HHO, with minimal overshoot, peak value, reduced rise, and settling time, outperforming the recently proposed controllers and additional cutting-edge controllers.

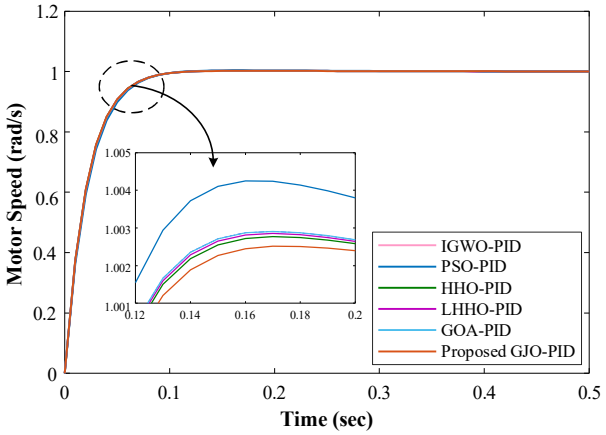

Figure 9 Comparison of the proposed GJO-PID with existing PID controllers regarding step responsiveness

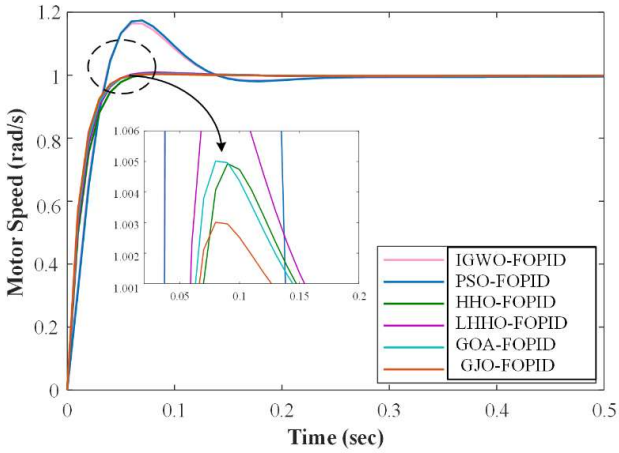

Figure 10 Comparison of the proposed GJO-FOPID with existing FOPID controllers regarding step responsiveness

C. Frequency Response Investigation

The study evaluates the frequency response of GJO-based PID- and FOPID-controlled DC motors against advanced algorithmic controllers, using Bode plots to assess stability. Key metrics include gain margin, which indicates the maximum gain before instability, and phase margin, which measures the phase adjustment needed for stability. Bandwidth indicates the effective frequency-response range, while crossover frequency marks the point at which the open-loop response is 0 dB. Figures 11 and 12 present the Bode plots of the GJO- and LHHO-based controllers, respectively, and Figure 13 presents the Bode plot of the proposed controller alongside the other controllers considered. Table 6 highlights the superior gain and phase margins, bandwidth, and crossover frequency of the proposed GJO controllers compared with the benchmark.

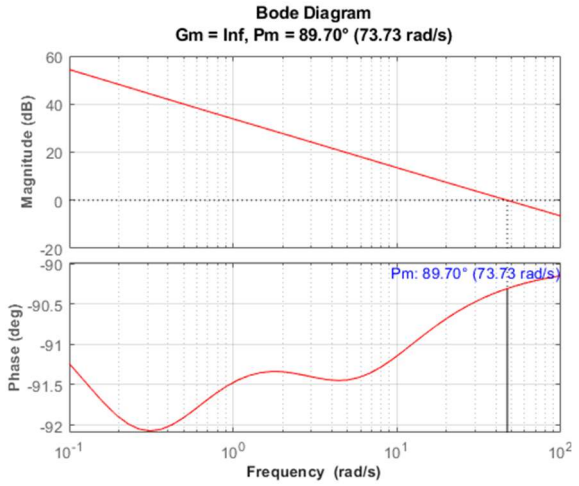

(a)

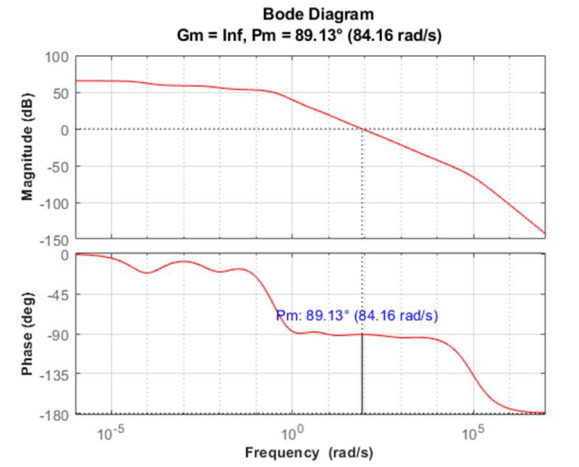

(b)

Figure 11 Bode plot for proposed (a) GJO-PID and (b) GJO-FOPID controller-based DC motor speed control system

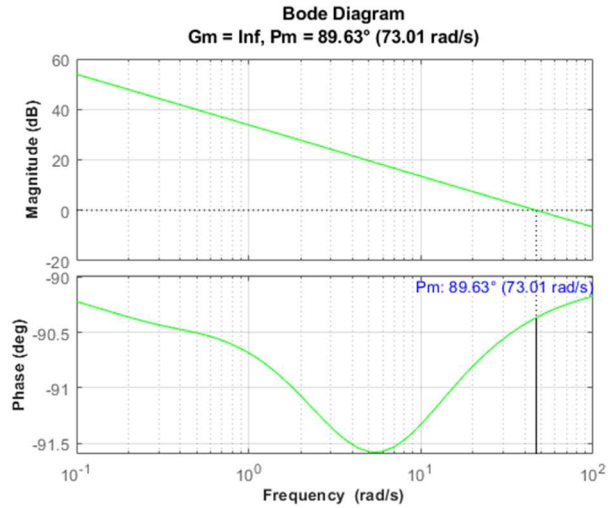

(a)

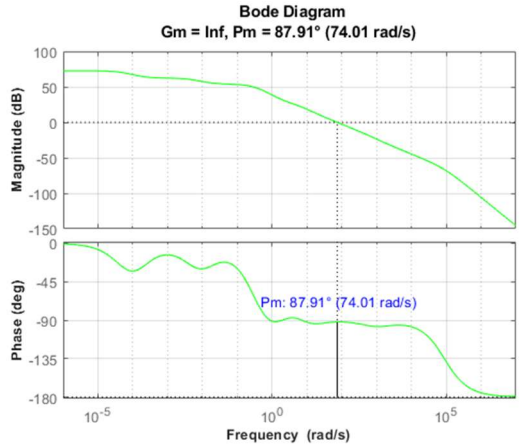

(b)

Figure 12 Bode plot for proposed (a) LHHO-PID and (b) LHHO-FOPID controller-based DC motor speed control

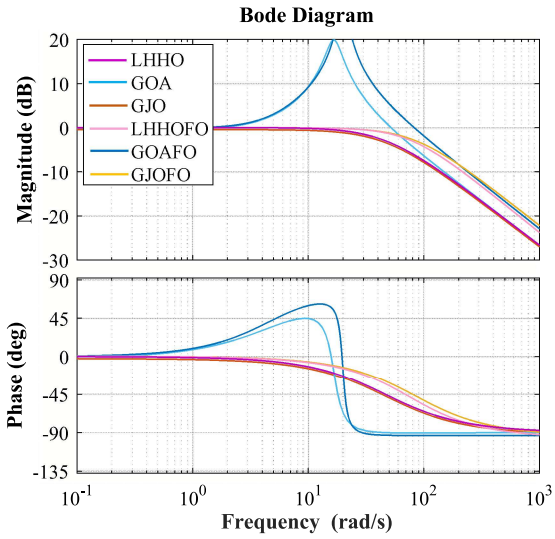

Figure 13 Bode plot of DC motor speed control for combined GJO-PID/FOPID, LHHO-PID/FOPID, and GOA-PID/FOPID controllers

Table 6 Analyze the frequency response results under various controller approaches

#	Algorithm	Gain-margin (dB)	Band width (Hz)	Phase margin (degree)	Phase crossover frequency (rad/s)
1	IGWO-PID (Li et al., 2021)	Infinite	46.839	89.626	46.647
2	PSO-PID (Rahayu et al., 2022)	Infinite	46.214	89.499	45.923
3	HHO-PID (Ekinci et al., 2020)	Infinite	47.004	89.653	46.832
4	LHHO-PID (Ayinla et al., 2024)	Infinite	46.856	89.634	46.669
5	GOA-PID (Izci &	Infinite	46.877	89.629	46.687

	Ekinci, 2023)				
6	GJO-PID (Proposed)	Infinite	47.235	89.696	47.096
7	IGWO-FOPID (Li et al., 2021)	Infinite	69.908	61.298	49.565
8	PSO-FOPID (Rahayu et al., 2022)	Infinite	68.487	60.014	48.211
9	HHO-FOPID (Munagala & Jatoth, 2021)	Infinite	70.274	88.674	68.756
10	LHHO-FOPID (Ayinla et al., 2024)	Infinite	76.590	87.914	74.0091
11	GOA-FOPID (Izci & Ekinci, 2023)	Infinite	80.327	88.718	78.667
12	GJO-FOPID (Proposed)	Infinite	85.351	89.129	84.165

The Bode plot analysis shows that all controllers, including the proposed GJO PID and FOPID, achieved infinite gain, indicating robustness against destabilization. The GJO algorithms have phase margins of 89.70° and 89.13° for PID and FOPID, respectively, outperforming other methods. The GJO-PID achieves the highest bandwidth at 47.23 Hz, while GJO-FOPID leads with 85.35 Hz. Other controllers follow with lower bandwidths: HHO-PID (47.00 Hz), GOA-FOPID (80.33 Hz), and the lowest being PSO-FOPID (68.49 Hz), which is significantly lower than GJO-FOPID. These results highlight GJO's superior stability and performance.

Furthermore, Phase Crossover Frequency (ω_{pc}), the frequency at which the open-loop system phase reaches −180° is a key indicator of stability and response speed. A higher ω_{pc} generally implies faster system dynamics. As shown in Table 6, the proposed GJO-PID and GJO-FOPID controllers achieve exceptional phase crossover frequencies of 47.10 rad/s and 84.17 rad/s, respectively. Compared to other FOPID controllers, the GJO-FOPID outperforms IGWO-FOPID, PSO-FOPID, HHO-FOPID, LHHO-FOPID, and GOA-FOPID by 34.60, 35.95, 15.41, 10.16, and 5.50 rad/s, respectively. These results, combined with high phase margins (~89°), demonstrate that the proposed controllers offer excellent stability and rapid dynamic response, making them highly effective for precise DC motor control. The observed infinite gain margin indicates that the magnitude response does not cross the 0 dB line at the phase crossover frequency.

D. Sensitivity Analysis

Sensitivity analysis evaluates controller stability and performance under disturbances. In this study, the sensitivity of the proposed GJO-PID and GJO-FOPID-based DC motor controller is assessed through the introduction of ±20% and ±30% variations in the armature inductance (L_a) and ±10% and ±25%, deviations in the torque constant (M_m) amounting to seven distinctive scenarios, as outlined in Table 7.

Table 7 Different operating conditions of the DC motor parameters

Cases No	Parameters	
	L_a	M_m
1	2.16	0.00135
2	2.16	0.00165
3	3.24	0.00135
4	3.24	0.00165
5	1.89	0.01125
6	1.89	0.01875
7	3.51	0.01125

The sensitivity of the proposed controller to uncertainties was assessed under the specified conditions by monitoring step and frequency variations. The findings indicated that the suggested controllers remain stable and efficient under various operating conditions, as depicted in Tables 8 and 9, under case study 1. Additionally, step-response and frequency-response performance for Cases 2-7 are summarized in Appendix Tables A1–A6 and B1–B6, respectively.

Detailed data analysis in these tables demonstrates the proposed controllers' efficient performance in assessing step and frequency responses across all considered parameter variations. Across all seven cases, the GJO-based PID and FOPID controllers consistently achieved the lowest rise time, settling time, overshoot, and steady-state error in the time domain, while also providing superior frequency-domain characteristics, including higher bandwidth and phase margin. These results confirm that the GJO controllers exhibit the fastest and most stable dynamic performance among the optimization-based controllers, thereby validating their enhanced robustness and effectiveness. These outcomes confirm the controllers' ability to manage speed control effectively, maintaining optimal performance despite uncertainties and parameter variations in the DC motor system.

Table 8 Step response performance under case 1 when $L_a = 2.16$ and $M_m = 0.0135$

#	Algorithm	t_r (s)	t_s (s)	O_p (%)	E_{SS}	p_v (rad/s)
1	IGWO-PID (Li et al., 2021)	0.0414	0.0715	0.2359	3.92e-4	1.0020
2	PSO-PID (Rahayu et al., 2022)	0.0419	0.0717	0.3181	1.78e-4	1.0030
3	HHO-PID (Ekinci et al., 2020)	0.0413	0.0715	0.2126	3.07e-4	1.0018
4	LHHO-PID (Ayinla et al., 2024)	0.0414	0.0715	0.2300	3.89e-4	1.0019
5	GOA-PID (Izci & Ekinci, 2023)	0.0414	0.0715	0.2325	3.63e-4	1.0020
6	GJO-PID (Proposed)	0.0411	0.0715	0.1779	2.03e-4	1.0016

7	IGWO-FOPID (Li et al., 2021)	0.0250	0.1213	16.6814	0.0044	1.1616
8	PSO-FOPID (Rahayu et al., 2022)	0.0254	0.1221	17.544	0.0044	1.1702
9	HHO-FOPID (Munagala & Jatoth, 2021)	0.0272	0.0460	0.6099	0.00161	1.0045
10	LHHO-FOPID (Ayinla et al., 2024)	0.0253	0.0402	0.9369	0.0016	1.0073
11	GOA-FOPID (Izci & Ekinci, 2023)	0.0244	0.0398	0.6093	0.0015	1.0046
12	GJO-FOPID (Proposed)	0.0232	0.0389	0.4102	0.0014	1.0027

Table 9 Frequency response performance under case 1 when $L_a = 2.16$ and $M_m = 0.0135$

#	Algorithm	Gain margin (dB)	Band width (Hz)	Phase margin (degree)	Phase crossover frequency (rad/s)
1	IGWO-PID (Li et al., 2021)	Infinite	52.61	89.70	52.4709
2	PSO-PID (Rahayu et al., 2022)	Infinite	51.89	89.595	51.6541
3	HHO-PID (Ekinci et al., 2020)	Infinite	52.80	89.73	52.6798
4	LHHO-PID (Ayinla et al., 2024)	Infinite	52.63	89.71	52.4959
5	GOA-PID (Izci & Ekinci, 2023)	Infinite	52.65	89.71	52.5157
6	GJO-PID (Proposed)	Infinite	53.06	89.76	52.9786
7	IGWO-FOPID (Li et al., 2021)	Infinite	76.79	62.27	54.4249
8	PSO-FOPID (Rahayu et al., 2022)	Infinite	75.12	61.01	52.8553
9	HHO-FOPID (Munagala & Jatoth, 2021)	Infinite	79.00	88.73	77.3640
10	LHHO-FOPID (Ayinla et al., 2024)	Infinite	86.09	87.96	83.2375
11	GOA-FOPID (Izci & Ekinci, 2023)	Infinite	90.36	88.74	88.5145
12	GJO-FOPID (Proposed)	Infinite	96.06	89.12	94.7177

VI. CONCLUSION

The increasing complexity of industrial control methods has recently highlighted the need for an optimal, robust optimization algorithm to tune controller parameters. This study presented a novel metaheuristic-based optimal control approach inspired by the cooperative hunting behavior of Canis aureus, addressing the gap in applying GJO to DC motor speed regulation with PID and FOPID controllers. This study explores the ITAE error function, as reported in previous studies, to achieve the desired system response by optimizing controller design parameters. To verify and evaluate the effectiveness of the proposed controllers, they are benchmarked against recently proposed methods, including IGWO-PID/FOPID, PSO-PID/FOPID, HHO-PID/FOPID, LHHO-PID/FOPID, and GOA-PID/FOPID. The proposed GJO-FOPID controller outperforms LHHO-FOPID by achieving a 6.98% faster rise time, a 4.10% shorter settling time, and a 0.56% lower overshoot, and surpasses GOA-FOPID by 3.87%, 3.42%, and 0.2022%, respectively, demonstrating superior dynamic performance. Additionally, both stability response and sensitivity analyses demonstrate competitive performance. In the future, this tuning method could be employed in more complex control systems and the presence of highly varying disturbances. Future work could also extend the present analysis to include load torque disturbances to evaluate the disturbance-rejection capability of the optimized controllers under realistic operating conditions.

AUTHOR CONTRIBUTIONS

M. G. Mostafa contributed to conceptualization, methodology, and writing – original draft; **Nor Zaihar B. Yahaya and R. Kannan** were responsible for supervision, validation, and writing – review & editing; **I. Shuaibu and M. S. Akter** assisted with research analysis and report review; all authors had approved the final version.

ACKNOWLDGEMENT

This research is conducted under the sponsorship of Universiti Teknologi PETRONAS (UTP), Perak, Malaysia, under the Graduate Assistantship (GA) scheme.

REFERENCES

Agarwal, J., Parmar, G., Gupta, R., & Sikander, A. (2018). Analysis of grey wolf optimizer based fractional order PID controller in speed control of DC motor. *Microsystem Technologies*, *24*(12), 4997-5006. https://doi.org/10.1007/s00542-018-3920-4.

Akter, K., Motakabeer, S. M. A., Zahirul Alam, A. H. M., & Jadoun, V. K. (2025). A novel MPPT approach for photovoltaic system using Pelican optimization and high-gain DC–DC converter. *Scientific Reports*, *15*(1), 40451. https://doi.org/10.1038/s41598-025-24000-z

Ayinla, L. S., Aziz, A. A., Drieberg, M., Azubogu, A. C., & Amosa, T. I. (2022). Energy management algorithm in wireless sensor network for pipeline monitoring. 2022 International Conference on Future Trends in Smart Communities (ICFTSC).

Ayinla, S. L., Amosa, T. I., Ibrahim, O., Rahman, M. S., Bahashwan, A. A., Mostafa, M. G., & Yusuf, A. O. (2024). Optimal control of DC motor using leader-based Harris Hawks optimization algorithm. *Franklin open*, *6*, 100058. https://doi.org/10.1016/j.fraope.2023.100058.

Ayinla, S. L., Amosa, T. I., Rahman, M. S., Owonikoko, W., Rahman, M. A., Barua, S., Rahman, T.,

& Liou, M. S. H. (2023). Optimizing DC Motor Control via Leader Harris Hawks Algorithm with ITSE-ZLG Objective Function. 2023 10th IEEE International Conference on Power Systems (ICPS),

Chopra, N., & Ansari, M. M. (2022). Golden jackal optimization: A novel nature-inspired optimizer for engineering applications. *Expert Systems with Applications*, *198*, 116924. https://doi.org/10.1016/j.eswa.2022.116924

Das, S., Saha, S., Das, S., & Gupta, A. (2011). On the selection of tuning methodology of FOPID controllers for the control of higher order processes. *ISA transactions*, *50*(3), 376-388. https://doi.org/10.1016/j.isatra.2011.02.003

Eker, E., Kayri, M., Ekinci, S., & Izci, D. (2021). A new fusion of ASO with SA algorithm and its applications to MLP training and DC motor speed control. *Arabian Journal for Science and Engineering*, *46*(4), 3889-3911. https://doi.org/10.1007/s13369-020-05228-5

Ekinci, S., Hekimoğlu, B., & Izci, D. (2021). Opposition based Henry gas solubility optimization as a novel algorithm for PID control of DC motor. *Engineering Science and Technology, an International Journal*, *24*(2), 331-342. https://doi.org/10.1016/j.jestch.2020.08.011

Ekinci, S., Izci, D., & Hekimoğlu, B. (2020). PID speed control of DC motor using Harris hawks optimization algorithm. 2020 International conference on electrical, communication, and computer engineering (ICECCE). https://doi.org/10.1109/ICECCE49384.2020.9179308

Hekimoğlu, B. (2019). Optimal tuning of fractional order PID controller for DC motor speed control via chaotic atom search optimization algorithm. *IEEE Access*, *7*, 38100-38114. https://doi.org/10.1109/ACCESS.2019.2905961

Ibrahim, M. A., Mahmood, A. K., & Sultan, N. S. (2019). Optimal PID controller of a brushless DC motor using genetic algorithm. *Int J Pow Elec & Dri Syst ISSN*, *2088*(8694), 8694. https://doi.org/10.11591/ijpeds.v10.i2.pp822-830

Islam, J., Meraj, S. T., Masaoud, A., Mahmud, M. A., Nazir, A., Kabir, M. A., Hossain, M. M., & Mumtaz, F. (2021). Opposition-based quantum bat algorithm to eliminate lower-order harmonics of multilevel inverters. *IEEE Access*, *9*, 103610-103626. https://doi.org/10.1109/ACCESS.2021.3098190

Issa, M. (2023). Enhanced arithmetic optimization algorithm for parameter estimation of PID controller. *Arabian Journal for Science and Engineering*, *48*(2), 2191-2205. https://doi.org/10.1007/s13369-022-07136-2

Izci, D., & Ekinci, S. (2023). Fractional order controller design via gazelle optimizer for efficient speed regulation of micromotors. *e-Prime-Advances in Electrical Engineering, Electronics and Energy*, *6*, 100295. https://doi.org/https://doi.org/10.1016/j.prime.2023.100295

Kumar, L., Pandey, M., & Ahirwal, M. K. (2023). Parallel global best-worst particle swarm optimization algorithm for solving optimization problems. *Applied Soft Computing*, *142*, 110329. https://doi.org/10.1016/j.asoc.2023.110329

Kumari, S., & Kumar, R. (2023). Hybridized GWO-RUN optimized fractional order control for permanent magnet brush-less dc motor. *Engineering Research Express*, *5*(1), 015056. https://doi.org/https://doi.org/doi:10.1088/2631-8695/acb896

Li, L.-L., Liu, J.-Q., Zhao, W.-B., & Dong, L. (2021). Fault diagnosis of high-speed brushless permanent-magnet DC motor based on support vector machine optimized by modified grey wolf optimization algorithm. *Symmetry*, *13*(2), 163. https://doi.org/https://doi.org/10.3390/sym13020163

Mantegna, R. N. (1994). Fast, accurate algorithm for numerical simulation of Levy stable stochastic processes. *Physical Review E*, *49*(5), 4677. https://doi.org/10.1103/PhysRevE.49.4677

Meraj, S. T., Hasan, K., & Masaoud, A. (2020). Design and application of SPWM based 21-level hybrid inverter for induction motor drive. *Turkish Journal of Electrical Engineering and Computer Sciences*, *28*(6), 3219-3234. https://doi.org/10.3906/elk-1901-8

Mosaad, A. M., Attia, M. A., Elbehairy, N. M., Alruwaili, M., Yousef, A., & Hamed, N. M. (2025). Enhancing AVR System Stability Using Non-Monopolize Optimization for PID and PIDA Controllers. *Processes*, *13*(10), 3072. https://doi.org/10.3390/pr13103072

Mostafa, M. G., Ibrahim, T. B., & Kannan, R. (2024). Hybrid Energy Harvesting System Optimization in the Oil and Gas Industry via Harris Hawks Optimization Technique. 2024 IEEE 6th Symposium on Computers & Informatics (ISCI).

Mostafa, M. G., Motakabber, S. M., Ibrahimy, M. I., & Rahman, T. (2006). Development of Piezoelectric Micro-energy Harvesting System Using Voltage Doubler. ARPN Journal of Engineering and Applied Sciences, 11(1), 351-355.

Munagala, V. K., & Jatoth, R. K. (2021). Design of fractional-order PID/PID controller for speed control of DC motor using Harris Hawks optimization. *Intelligent algorithms for analysis and control of dynamical systems*, 103-113. https://doi.org/10.1007/978-981-15-8045-1_11

Podlubny, I. (1994). Fractional-order systems and fractional-order controllers. *Institute of Experimental Physics, Slovak Academy of Sciences, Kosice*, *12*(3), 1-18. https://doi.org/10.3390/fractalfract7010048

Qaraad, M., Amjad, S., Hussein, N. K., Farag, M., Mirjalili, S., & Elhosseini, M. A. (2024). Quadratic interpolation and a new local search approach to improve particle swarm optimization: Solar photovoltaic parameter estimation. Expert Systems with Applications, 236, 121417. https://doi.org/10.1016/j.eswa.2023.121417

Rahayu, E. S., Ma'arif, A., & Cakan, A. (2022). Particle Swarm Optimization (PSO) Tuning of PID Control on DC Motor. *International Journal of Robotics & Control Systems*, *2*(2). https://doi.org/https://doi.org/10.31763/ijrcs.v2i2.476

Shuaibu, I., Wei, E. H. T., Kannan, R., & Samaila, Y. A. (2024). Advancements in axial flux permanent magnet machines utilizing coreless technology: A systematic review. Ain Shams Engineering Journal, 15(12), 103091. https://doi.org/ 10.1016/j.asej.2024.103091

Suman, S. K., & Giri, V. K. (2016). Genetic algorithms techniques based optimal PID tuning for speed control of DC motor. *American Journal of Engineering and Technology Management*, *1*(4), 59-64. https://doi.org/10.11648/j.ajetm.20160104.12

Younus, S. M. Y., Kutbay, U., Rahebi, J., & Hardalaç, F. (2023). Hybrid gray wolf optimization–proportional integral based speed controllers for brush-less dc motor. *Energies*, *16*(4), 1640. https://doi.org/10.3390/en16041640

APPENDIX

Step-response performance under Cases 2-7 is summarized in Tables A1–A6, which present rise time, settling time, overshoot, and steady state error. Frequency-domain behavior is quantified in Tables B2-B6, which present gain margin, bandwidth, phase margin, and Phase crossover frequency under Cases 2-7, respectively.

Table A1 Step response performance under case 2 when $L_a = 2.16$ and $M_m = 0.0165$

#	Algorithm	t_r (s)	t_s (s)	O_p (%)	E_{SS}	p_v (rad/s)
1	IGWO-PID (Li et al., 2021)(Li et al., 2021)	0.0341	0.0588	0.2420	7.39e-04	1.0017
2	PSO-PID (Rahayu et al., 2022)(Rahayu et al., 2022)	0.0345	0.0590	0.3167	5.68e-04	1.0026
3	HHO-PID (Ekinci et al., 2020)(Ekinci et al., 2020)	0.0340	0.0588	0.2208	6.67e-04	1.0015
4	LHHO-PID (Ayinla et al., 2024)(Ayinla et al., 2024)	0.0341	0.0588	0.2367	7.37e-04	1.0016
5	GOA-PID (Izci & Ekinci, 2023)(Izci & Ekinci, 2023)	0.0341	0.0588	0.2389	7.14e-04	1.0017
6	GJO-PID (Proposed)	0.0339	0.0588	0.1881	5.77e-04	1.0013
7	IGWO-FOPID (Li et al., 2021)(Li et al., 2021)	0.0217	0.1099	15.673	0.00380	1.1523
8	PSO-FOPID (Rahayu et al., 2022)(Rahayu et al., 2022)	0.0222	0.1104	16.455	0.00379	1.1601
9	HHO-FOPID (Munagala & Jatoth, 2021)(Munagala & Jatoth, 2021)	0.0229	0.0382	0.6108	0.00158	1.0045
10	LHHO-FOPID (Ayinla et al., 2024)(Ayinla et al., 2024)	0.0206	0.0345	0.8870	0.00156	1.0073
11	GOA-FOPID (Izci & Ekinci, 2023)(Izci & Ekinci, 2023)	0.0194	0.0340	0.5841	0.00144	1.0044
12	GJO-FOPID (Proposed)	0.0182	0.0325	0.3999	0.00139	1.0026

Table A2 Step response performance under case 3 when $L_a = 3.24$and $M_m = 0.0135$

#	Algorithm-	t_r (s)	t_s (s)	O_p (%)	E_{SS}	p_v (rad/s)
1	IGWO-PID (Li et al., 2021)(Li et al., 2021)	0.0619	0.1066	0.2203	0.002114	1.0043
2	PSO-PID (Rahayu et al., 2022)(Rahayu et al., 2022)	0.0625	0.1065	0.3108	0.002461	1.0056
3	HHO-PID (Ekinci et al., 2020)(Ekinci et al., 2020)	0.0618	0.1067	0.1963	0.002229	1.0042
4	LHHO-PID (Ayinla et al., 2024)(Ayinla et al., 2024)	0.0619	0.1067	0.2141	0.002117	1.0043
5	GOA-PID (Izci & Ekinci, 2023)(Izci & Ekinci, 2023)	0.06189	0.1066	0.2170	0.002154	1.0043
6	GJO-PID (Proposed)	0.0616	0.1069	0.1591	0.002372	1.0040
7	IGWO-FOPID (Li et al., 2021)(Li et al., 2021)	0.0334	0.2036	18.4657	0.005612	1.1780
8	PSO-FOPID (Rahayu et al., 2022)(Rahayu et al., 2022)	0.0338	0.2193	19.3538	0.005606	1.1868
9	HHO-FOPID (Munagala & Jatoth, 2021)(Munagala & Jatoth, 2021)	0.0405	0.0666	0.5310	7.0470e-04	1.0046
10	LHHO-FOPID (Ayinla et al., 2024)(Ayinla et al., 2024)	0.0366	0.0587	0.9542	8.9810e-04	1.0086
11	GOA-FOPID (Izci & Ekinci, 2023)(Izci & Ekinci, 2023)	0.0356	0.0586	0.5853	7.0737e-04	1.0051
12	GJO-FOPID (Proposed)	0.0340	0.0572	0.3715	6.8498e-04	1.0030

Table A3 Step response performance under case 4 when $L_a = 3.24$ and $M_m = 0.0165$

#	Algorithm	t_r (s)	t_s (s)	O_p (%)	E_{SS}	p_v (rad/s)
1	IGWO-PID (Li et al., 2021)(Li et al., 2021)	0.0507	0.0875	0.2381	0.0013	1.003
2	PSO-PID (Rahayu et al., 2022)(Rahayu et al., 2022)	0.0513	0.0876	0.3262	0.00156	1.004
3	HHO-PID (Ekinci et al., 2020)(Ekinci et al., 2020)	0.0506	0.0876	0.2137	0.0015	1.003

4	LHHO-PID (Ayinla et al., 2024)(Ayinla et al., 2024)	0.0507	0.0876	0.2319	0.0013	1.003
5	GOA-PID (Izci & Ekinci, 2023)(Izci & Ekinci, 2023)	0.0507	0.0875	0.2347	0.0013	1.003
6	GJO-PID (Proposed)	0.0504	0.0877	0.1773	0.0015	1.003
7	IGWO-FOPID (Li et al., 2021)(Li et al., 2021)	0.0289	0.1344	17.644	0.0047	1.170
8	PSO-FOPID (Rahayu et al., 2022)(Rahayu et al., 2022)	0.0295	0.1353	18.536	0.0046	1.179
9	HHO-FOPID (Munagala & Jatoth, 2021)(Munagala & Jatoth, 2021)	0.0336	0.0554	0.5996	8.1e-04	1.005
10	LHHO-FOPID (Ayinla et al., 2024)(Ayinla et al., 2024)	0.0304	0.0489	0.9720	9.3e-04	1.008
11	GOA-FOPID (Izci & Ekinci, 2023)(Izci & Ekinci, 2023)	0.0289	0.0487	0.6203	7.9e-04	1.005
12	GJO-FOPID (Proposed)	0.0275	0.0475	0.4091	7.7e-04	1.003

Table A4: Step response performance under case 5 when $L_a = 1.89$ and $M_m = 0.01125$

#	Algorithm	t_r (s)	t_s (s)	O_p (%)	E_{SS}	p_v (rad/s)
1	IGWO-PID (Li et al., 2021)(Li et al., 2021)	0.0435	0.0754	0.2287	7.5e-4	1.0015
2	PSO-PID (Rahayu et al., 2022)(Rahayu et al., 2022)	0.0440	0.0755	0.3105	5.2e-4	1.0026
3	HHO-PID (Ekinci et al., 2020)(Ekinci et al., 2020)	0.0434	0.0754	0.2055	6.5e-4	1.0014
4	LHHO-PID (Ayinla et al., 2024)(Ayinla et al., 2024)	0.0435	0.0754	0.2228	7.4e-4	1.0015
5	GOA-PID (Izci & Ekinci, 2023)(Izci & Ekinci, 2023)	0.0435	0.0753	0.2310	7.3e-4	1.0016
6	GJO-PID (Proposed)	0.0432	0.0754	0.1696	5.4e-4	1.0012
7	IGWO-FOPID (Li et al., 2021)(Li et al., 2021)	0.0257	0.1245	16.8590	0.0048	1.1629
8	PSO-FOPID (Rahayu et al., 2022)(Rahayu et al., 2022)	0.0261	0.1252	17.6542	0.0048	1.1709
9	HHO-FOPID (Munagala & Jatoth, 2021)(Munagala & Jatoth, 2021)	0.0281	0.0479	0.6126	0.0019	1.0042
10	LHHO-FOPID (Ayinla et al., 2024)(Ayinla et al., 2024)	0.0263	0.0427	0.9528	0.0019	1.0076
11	GOA-FOPID (Izci & Ekinci, 2023)(Izci & Ekinci, 2023)	0.0255	0.0423	0.6137	0.0017	1.0044
12	GJO-FOPID (Proposed)	0.0243	0.0403	0.4115	0.0017	1.0024

Table A5 Step response performance under case 6 when $L_a = 1.89$ and $M_m = 0.01875$

#	Algorithm	t_r (s)	t_s (s)	O_p (%)	E_{SS}	p_v (rad/s)
1	IGWO-PID (Li et al., 2021)(Li et al., 2021)	0.0263	0.0461	0.2407	0.001360	1.0010
2	PSO-PID (Rahayu et al., 2022)(Rahayu et al., 2022)	0.0266	0.0464	0.3066	0.001232	1.0018
3	HHO-PID (Ekinci et al., 2020)(Ekinci et al., 2020)	0.0262	0.0461	0.2217	0.001302	1.0009
4	LHHO-PID (Ayinla et al., 2024)(Ayinla et al., 2024)	0.0263	0.0462	0.2360	0.001359	1.0010
5	GOA-PID (Izci & Ekinci, 2023)(Izci & Ekinci, 2023)	0.0263	0.0461	0.2425	0.001351	1.0011
6	GJO-PID (Proposed)	0.0262	0.0460	0.1924	0.001230	1.0007
7	IGWO-FOPID (Li et al., 2021)(Li et al., 2021)	0.0173	0.0976	14.3262	0.003260	1.1395
8	PSO-FOPID (Rahayu et al., 2022)(Rahayu et al., 2022)	0.0176	0.0979	15.0427	0.003256	1.1467
9	HHO-FOPID (Munagala & Jatoth, 2021)(Munagala & Jatoth, 2021)	0.0175	0.0295	0.5769	0.001748	1.0040
10	LHHO-FOPID (Ayinla et al., 2024)(Ayinla et al., 2024)	0.0166	0.0275	0.7989	0.001679	1.0063

11	GOA-FOPID (Izci & Ekinci, 2023)(Izci & Ekinci, 2023)	0.0161	0.0272	0.5267	0.001579	1.0037
12	GJO-FOPID (Proposed)	0.0155	0.0263	0.3666	0.001524	1.0021

Table A6 Step response performance under case 7 when $L_a = 3.51$ and $M_m = 0.01125$

#	Algorithm	t_r (s)	t_s (s)	O_p (%)	E_{SS}	p_v
1	IGWO-PID (Li et al., 2021)(Li et al., 2021)	0.0803	0.1379	0.182	0.0038	1.0057
2	PSO-PID (Rahayu et al., 2022)(Rahayu et al., 2022)	0.0810	0.1375	0.267	0.0043	1.0070
3	HHO-PID (Ekinci et al., 2020)(Ekinci et al., 2020)	0.0802	0.1382	0.159	0.0039	1.0056
4	LHHO-PID (Ayinla et al., 2024)(Ayinla et al., 2024)	0.0803	0.1381	0.175	0.0038	1.0056
5	GOA-PID (Izci & Ekinci, 2023)(Izci & Ekinci, 2023)	0.0803	0.1379	0.184	0.0038	1.005
6	GJO-PID (Proposed)	0.0800	0.1386	0.125	0.0041	1.005
7	IGWO-FOPID (Li et al., 2021)(Li et al., 2021)	0.0401	0.2596	19.274	0.0071	1.184
8	PSO-FOPID (Rahayu et al., 2022)(Rahayu et al., 2022)	0.0406	0.2655	20.041	0.0072	1.191
9	HHO-FOPID (Munagala & Jatoth, 2021)(Munagala & Jatoth, 2021)	0.0521	0.0850	0.393	3.7e-4	1.003
10	LHHO-FOPID (Ayinla et al., 2024)(Ayinla et al., 2024)	0.0468	0.0748	0.847	6.9e-4	1.008
11	GOA-FOPID (Izci & Ekinci, 2023)(Izci & Ekinci, 2023)	0.0457	0.0750	0.499	4.2e-4	1.005
12	GJO-FOPID (Proposed)	0.0437	0.0731	0.290	3.9e-4	1.002

Table B1 Frequency response performance under case 2 when $L_a = 2.16$ and $M_m = 0.0165$

#	Algorithm	Gain margin (dB)	Band width (Hz)	Phase margin (degree)	Phase crossover frequency (rad/s)
1	IGWO-PID (Li et al., 2021)(Li et al., 2021)	Infinite	64.23	89.7598	64.12
2	PSO-PID (Rahayu et al., 2022)(Rahayu et al., 2022)	Infinite	63.33	89.6674	63.12
3	HHO-PID (Ekinci et al., 2020)(Ekinci et al., 2020)	Infinite	64.47	89.7793	64.38
4	LHHO-PID (Ayinla et al., 2024)(Ayinla et al., 2024)	Infinite	64.26	89.7655	64.15
5	GOA-PID (Izci & Ekinci, 2023)(Izci & Ekinci, 2023)	Infinite	64.28	89.7620	64.17
6	GJO-PID (Proposed)	Infinite	64.80	89.8104	64.74
7	IGWO-FOPID (Li et al., 2021)(Li et al., 2021)	Infinite	90.78	63.6661	64.14
8	PSO-FOPID (Rahayu et al., 2022)(Rahayu et al., 2022)	Infinite	88.58	62.4856	62.14
9	HHO-FOPID (Munagala & Jatoth, 2021)(Munagala & Jatoth, 2021)	Infinite	96.64	88.7180	94.60
10	LHHO-FOPID (Ayinla et al., 2024)(Ayinla et al., 2024)	Infinite	1e+02	87.9023	101.69
11	GOA-FOPID (Izci & Ekinci, 2023)(Izci & Ekinci, 2023)	Infinite	1e+02	88.6685	108.20
12	GJO-FOPID (Proposed)	Infinite	1e+02	89.0341	115.81

Table B2 Frequency response performance under case 3 when $L_a = 3.24$ and $M_m = 0.0135$

#	Algorithm	Gain margin (dB)	Band width (Hz)	Phase margin (degree)	Phase crossover frequency (rad/s)
1	IGWO-PID (Li et al., 2021)(Li et al., 2021)	Infinite	35.000	89.4656	35.24
2	PSO-PID(Rahayu et al., 2022)(Rahayu et al., 2022)	Infinite	34.802	89.2980	34.46
3	HHO-PID (Ekinci et al., 2020)(Ekinci et al., 2020)	Infinite	35.359	89.5007	35.13
4	LHHO-PID (Ayinla et al., 2024)(Ayinla et al., 2024)	Infinite	35.252	89.4758	35.01

5	GOA-PID (Izci & Ekinci, 2023)(Izci & Ekinci, 2023)	Infinite	35.270	89.4694	35.03
6	GJO-PID (Proposed)	Infinite	35.521	89.5568	35.33
7	IGWO-FOPID (Li et al., 2021)(Li et al., 2021)	Infinite	56.195	58.8213	39.82
8	PSO-FOPID (Rahayu et al., 2022)(Rahayu et al., 2022)	Infinite	55.234	57.5228	38.88
9	HHO-FOPID (Munagala & Jatoth, 2021)(Munagala & Jatoth, 2021)	Infinite	52.945	88.4276	51.60
10	LHHO-FOPID (Ayinla et al., 2024)(Ayinla et al., 2024)	Infinite	57.732	87.6682	55.59
11	GOA-FOPID (Izci & Ekinci, 2023)(Izci & Ekinci, 2023)	Infinite	60.3892	88.5687	59.00
12	GJO-FOPID (Proposed)	Infinite	64.0472	89.0571	63.08

Table B3: Frequency response performance under case 4 when $L_a = 3.24$ and $M_m = 0.0165$

#	Algorithm	Gain margin (dB)	Phase margin (degree)	Band width (Hz)	Phase crossover frequency (rad/s)
1	IGWO-PID (Li et al., 2021)(Li et al., 2021)	Infinite	89.560	42.990	42.76
2	PSO-PID (Rahayu et al., 2022)(Rahayu et al., 2022)	Infinite	89.560	42.990	42.76
3	HHO-PID (Ekinci et al., 2020)(Ekinci et al., 2020)	Infinite	89.589	43.138	42.93
4	LHHO-PID (Ayinla et al., 2024)(Ayinla et al., 2024)	Infinite	89.568	43.004	42.78
5	GOA-PID (Izci & Ekinci, 2023)(Izci & Ekinci, 2023)	Infinite	89.563	43.025	42.80
6	GJO-PID (Proposed)	Infinite	89.635	43.347	43.17
7	IGWO-FOPID (Li et al., 2021)(Li et al., 2021)	Infinite	60.541	65.341	46.32
8	PSO-FOPID (Rahayu et al., 2022)(Rahayu et al., 2022)	Infinite	59.245	64.079	45.11
9	HHO-FOPID (Munagala & Jatoth, 2021)(Munagala & Jatoth, 2021)	Infinite	88.605	64.484	63.0262
10	LHHO-FOPID (Ayinla et al., 2024)(Ayinla et al., 2024)	Infinite	87.851	70.288	67.8612
11	GOA-FOPID (Izci & Ekinci, 2023)(Izci & Ekinci, 2023)	Infinite	88.67	73.667	72.1054
12	GJO-FOPID (Proposed)	Infinite	89.11	78.236	77.1322

Table B4 Frequency response performance under case 5 when $L_a = 1.89$ and $M_m = 0.01125$

#	Algorithm	Gain margin (dB)	Band width (Hz)	Phase margin (degree)	Phase crossover frequency (rad/s)
1	IGWO-PID (Li et al., 2021)(Li et al., 2021)	Infinite	50.097	89.7235	49.97
2	PSO-PID (Rahayu et al., 2022)(Rahayu et al., 2022)	Infinite	49.418	89.6061	49.19
3	HHO-PID (Ekinci et al., 2020)(Ekinci et al., 2020)	Infinite	50.274	89.7483	50.17
4	LHHO-PID (Ayinla et al., 2024)(Ayinla et al., 2024)	Infinite	50.114	89.7308	49.99
5	GOA-PID (Izci & Ekinci, 2023)(Izci & Ekinci, 2023)	Infinite	50.098	89.7199	49.97

6	GJO-PID (Proposed)	Infinite	50.524	89.7877	50.45
7	IGWO-FOPID (Li et al., 2021)(Li et al., 2021)	Infinite	73.806	61.9243	52.34
8	PSO-FOPID (Rahayu et al., 2022)(Rahayu et al., 2022)	Infinite	72.246	60.6568	50.86
9	HHO-FOPID (Munagala & Jatoth, 2021)(Munagala & Jatoth, 2021)	Infinite	75.226	88.7485	73.67
10	LHHO-FOPID (Ayinla et al., 2024)(Ayinla et al., 2024)	Infinite	81.977	87.9768	79.28
11	GOA-FOPID (Izci & Ekinci, 2023)(Izci & Ekinci, 2023)	Infinite	86.022	88.7643	84.29
12	GJO-FOPID (Proposed)	Infinite	91.438	89.1594	90.19

Table B5 Frequency response performance under case 6 when $L_a = 1.89$ and $M_m = 0.01875$

#	Algorithm	Gain margin (dB)	Band width (Hz)	Phase margin (degree)	Phase crossover frequency (rad/s)
1	IGWO-PID (Li et al., 2021)(Li et al., 2021)	Infinite	83.306	89.832	83.26
2	PSO-PID (Rahayu et al., 2022)(Rahayu et al., 2022)	Infinite	82.100	89.761	81.95
3	HHO-PID (Ekinci et al., 2020)(Ekinci et al., 2020)	Infinite	83.619	89.847	83.59
4	LHHO-PID (Ayinla et al., 2024)(Ayinla et al., 2024)	Infinite	83.340	89.837	83.30
5	GOA-PID (Izci & Ekinci, 2023)(Izci & Ekinci, 2023)	Infinite	83.305	89.830	83.26
6	GJO-PID (Proposed)	Infinite	84.06	89.871	84.07
7	IGWO-FOPID (Li et al., 2021)(Li et al., 2021)	Infinite	1.1e+02	64.932	80.08
8	PSO-FOPID (Rahayu et al., 2022)(Rahayu et al., 2022)	Infinite	1.11e+02	63.893	77.34
9	HHO-FOPID (Munagala & Jatoth, 2021)(Munagala & Jatoth, 2021)	Infinite	1.26e+02	88.571	122.90
10	LHHO-FOPID (Ayinla et al., 2024)(Ayinla et al., 2024)	Infinite	1.37e+02	87.679	131.93
11	GOA-FOPID (Izci & Ekinci, 2023)(Izci & Ekinci, 2023)	Infinite	1.44e+02	88.468	140.49
12	GJO-FOPID (Proposed)	Infinite	1.53e+02	88.8275	150.40

Table B6 Frequency response performance under case 7 when $L_a = 3.51$ and $M_m = 0.01125$

#	Algorithm	Gain margin (dB)	Band width (Hz)	Phase margin (degree)	Phase crossover frequency (rad/s)
1	IGWO-PID (Li et al., 2021)(Li et al., 2021)	Infinite	27.207	89.2929	26.94
2	PSO-PID (Rahayu et al., 2022)(Rahayu et al., 2022)	Infinite	26.896	89.0790	26.53
3	HHO-PID (Ekinci et al., 2020)(Ekinci et al., 2020)	Infinite	27.290	89.3376	27.04
4	LHHO-PID (Ayinla et al., 2024)(Ayinla et al., 2024)	Infinite	27.213	89.3059	26.95
5	GOA-PID (Izci & Ekinci,	Infinite	27.209	89.2863	26.94

	2023)(Izci & Ekinci, 2023)				
6	GJO-PID (Proposed)	Infinite	27.405	89.4088	27.19
7	IGWO-FOPID (Li et al., 2021)(Li et al., 2021)	Infinite	46.629	56.6512	33.00
8	PSO-FOPID (Rahayu et al., 2022)(Rahayu et al., 2022)	Infinite	45.949	55.3925	32.32
9	HHO-FOPID (Munagala & Jatoth, 2021)(Munagala & Jatoth, 2021)	Infinite	41.079	88.0713	39.81
10	LHHO-FOPID (Ayinla et al., 2024)(Ayinla et al., 2024)	Infinite	44.848	87.2541	42.92
11	GOA-FOPID (Izci & Ekinci, 2023)(Izci & Ekinci, 2023)	Infinite	46.737	88.2869	45.46
12	GJO-FOPID (Proposed)	Infinite	49.443	88.8712	48.54